ÉCOLE POLYTECHNIQUE
FÉDÉRALE DE LAUSANNE

Laboratoire d'Algorithmes et Systemes
d'Apprentissage (LASA)
Prof. Aude Billard

EPFL, STI -
Faculte Sciences et Techniques de l'ingenieur
Institut d'ingenierie des systemes (I2S)

Design of a test-bed for a robotic satellite

Semester Project – Winter 2011

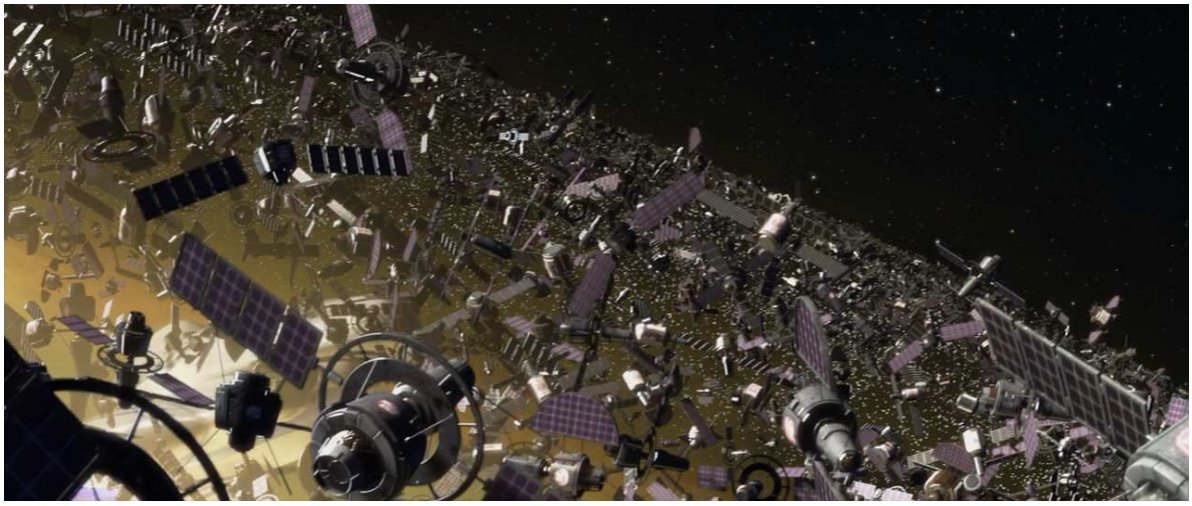

Laurent Blanchet
Exchange Student
ENS Cachan, Paris

Jean-Baptiste Keller
Reymond Clavel
Advisors

clean-m

LASA

Contents

1 Introduction

Due to mankind exploitation of space, many thousands of man-made objects are now in space. As we know, space is big and pretty much empty. However, due to mankind needs, the situation is very different in the vicinity of Earth. The situation degrades rapidly in Geostationary Earth Orbit (GEO) and worsen as we go toward Low Earth Orbit (LEO): there is still a lot of space, but for a first part the useful orbits are kind of the same, and there is a lot of objects due to the commercial use of those orbits (see figure 1).

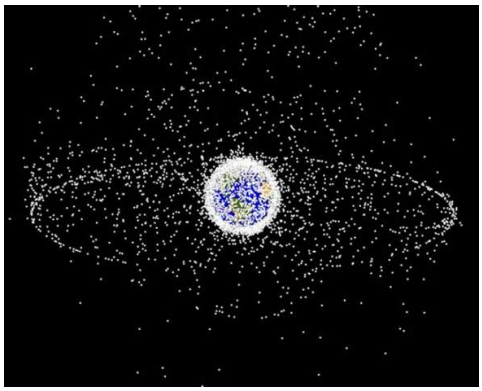

Figure 1: Objects >10cm in orbit: situation in 2010.

As of now, the situation is not good: satellites have to been armored to withstand small impacts from wandering fastenings, and have to be launched with large propellants tanks that will be used to avoid collisions with debris bigger than $10\,cm$. We can quote the example of the International Space Station (ISS), which orbit is really low in order to get it clear of debris. The energetic cost is high, and its orbit regularly needs to be raised. Even with this precaution, the ISS does collision avoidance manoeuvres all year long. Some debris are noticed too late to perform manoeuvres, and the people inhabiting the station have to get into the two Soyuz ships always docked to the station in case of emergency evacuation. Such a scenario happened on June, 28th 2011. The debris was at $250\,m$ from the station.

However contrary to the ISS, the satellites are not equipped to be serviced and when their tanks are empty, they are bound to collide with some other inert object in orbit and potentially create new inert objects (Kessler Syndrome) (see figure 2).

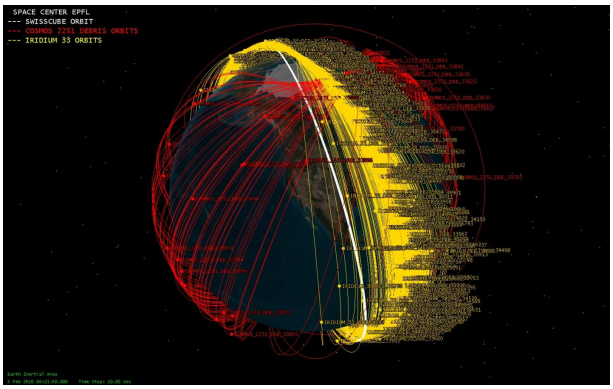

Figure 2: Collision event of Iridium and Cosmos satellites, situation in 2009. The red lines are tracked fragments of Cosmos, the yellow ones tracked fragments of Iridium.

The present situation is already a planned doom of space utilization: event without any

more launches, the already present debris will collide and the quantity of debris will overcome the quantity of useful payloads in orbit by 2050 in the most optimist prediction (NASA LEGEND forecasts) for debris of size superior than 10 cm. However the reality is worst: although the last years and the very short future did and will not see a lot of new launches due to the economic situation of the counties carrying the market of satellite and launchers, a study by the Northern Sky Research forecasts over 1600 new satellites built and launched by the year 2025 [1].

One overall question remains: what are those debris ? In the ideal situation where all satellites are de-orbited at the end of their lives, as specified by the regulations, instead of extending their mission until they can not be de-orbited, parts of the rocket stay in orbit, see figure 3. They are not only useless, but also very big and heavy.

The scientific community is reviewing different solutions, and developing technologies to upgrade their Technology Readiness Level (TRL). As for now the most feasible solution is to get a chaser satellite in orbit, grab the debris and de-orbit it.

The Space Center at EPFL is putting together an Orbital Debris Removal (ODR) mission. This project is called Clean-mE, see reference [2].

A previous thesis [3] in the framework of this project, has determined a scenario for the ODR mission and implemented a dynamic control using Yoshida's Generalized Jacobian [4]. In this thesis, we are concerned with the design of hardware allowing to dock a manipulator in a reaction-free fashion. This reaction-free test-bed has two purposes: first test the algorithm of the previous thesis with an actual KUKA's LWR and second, to emulate contact dynamics in the grabbing phase of the proposed scenario.

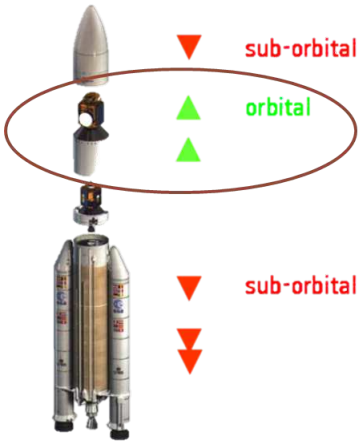

Figure 3: Parts of a rocket separated by post-deployment situation.

This thesis describes the design and configuration of the test-bed for robotic satellite and contact dynamics emulation. In this introduction, the ODR scenario is stated. Then, the difference between ground-based robotics and space robotics is highlighted and finally the problem addressed is detailed. Then the description moves on to each of the three subsystems of the test-bed, detailing architecture. It ends up with the tests carried out on a prototype of the Attitude Platform.

1.1 Scenario of the ODR mission

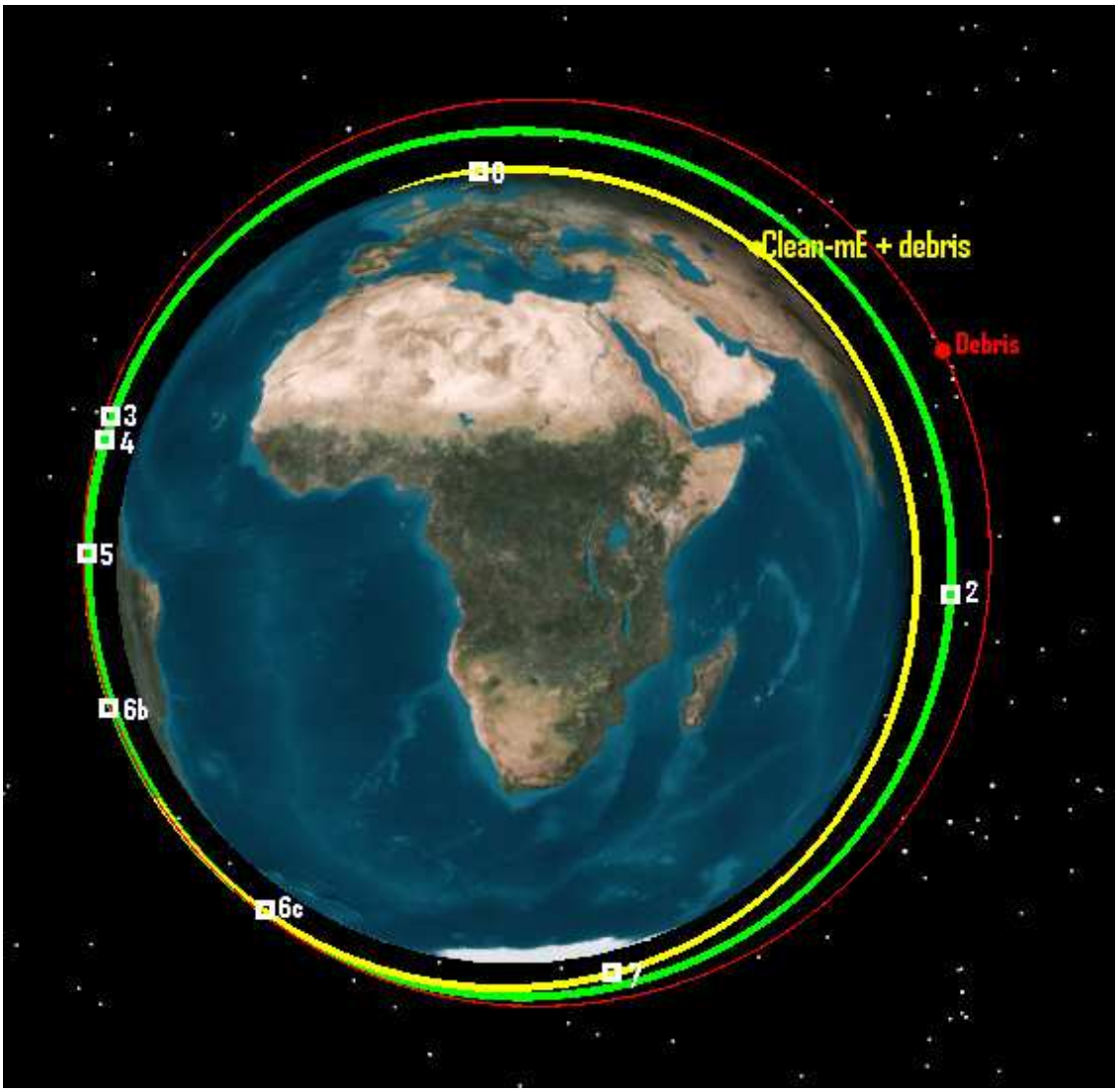

Figure 4: Deorbit scenario.

The goal of the ADCS + grabbing subsystem design is to reduce the use of the ADCS during the grabbing phase in order to reduce the consumption of fuels. The optimal reduction is to not use it at all. That is satisfied by the scenario of the mission as it follows (see figure 4):

1. Launch, deployments, orbit positioning (circular orbit below the target).
2. Analysis of the target (as many orbits as necessary, until the target is well identified, as well as its movements).
3. Rendezvous (closing gap between target and chaser: the chaser approach closer than one meter the target moving zone (see figure 5: the big black arrow is the axis of rotation of

the target, its origin is the center of mass. The target pictured is the H10 upper stage (Ariane 4), our main targets. The wide-spaced dotted frame depict the window in which the target moves, and that the chaser will avoid, the norrow-spaced dotted frame is the same window but for the x angle to 0 degrees (worst case)).

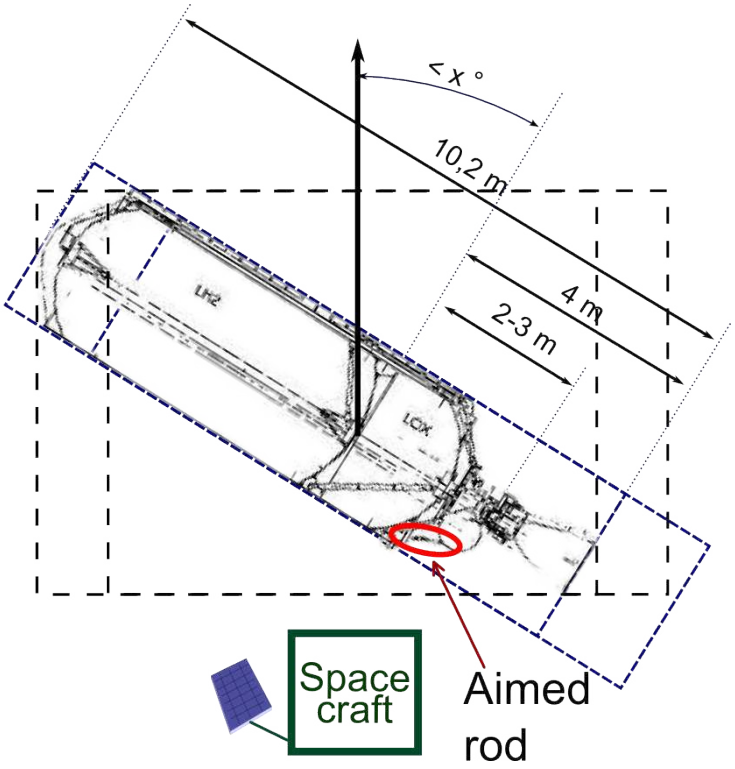

Figure 5: Approach and positioning of the chaser with reference to the target.

4. Emptying momentum of the reaction wheels (no perturbing reactions during catching phase that can be avoided! This phase can be done with the arm to save some fuel, see Longman's scenario for base attitude control in [5]. According to projections from the Yuki's scenario [6], the emptying of reaction wheels momentum is the task that use most of the on-board fuel).

5. Grabbing (see [3]): the chaser is placed within the axis of rotation of the target, and from there the arm follows the point aimed for the grabbing while the target rotates (see figure 5). This point aimed at for the grabbing phase is the middle of the exposed connecting rod between the LOX tank and the re-pressure tank.

6. Autonomous phase:

   (a) (passive sub-phase) Target grabbed, chaser adopts the movement of the target (inertia of the target way over the chaser's).

   (b) Reversing the kinematics, the chaser places itself onto the target, in a location that will allow it to control the trajectory, communicate with ground stations and have

an efficient thrust for the group formed by itself and the target (see figure 6).

The favoured scenario is the nozzle atop configuration. In this configuration, the alignment does not rely on the tanks-nozzle alignment because of two problems. First, as soon as the rocket's thrust is shut down, this alignment is disabled[1]. Second, after the burn, the geometrical definition of the nozzle is no longer known. Hence, the idea is to control the alignment *via* the robotic arm, still grabbing the rod, while the main thrust goes by the nozzle.

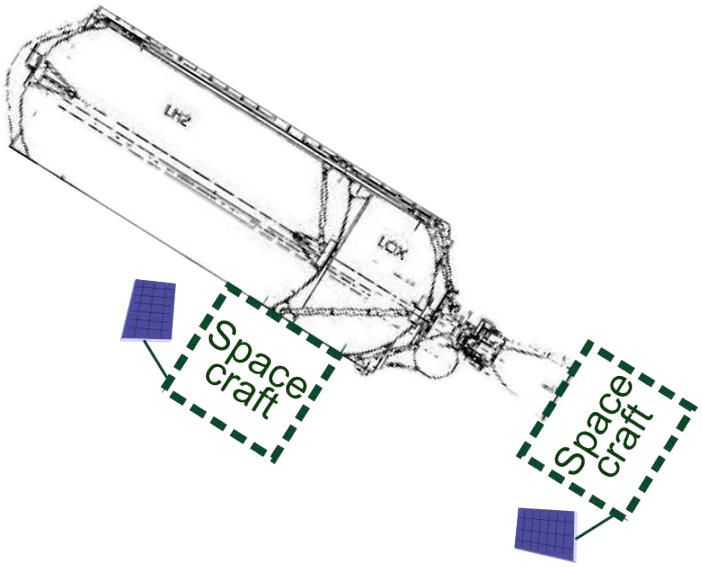

Figure 6: Detail of step 6b : two possible positions of the chaser onto the target. The reader's attention is directed towards the nozzle position: in this configuration, the chaser is aligned with the center of mass of the target by the manipulator still connected to the rod, it will produce an efficient thrust.

(c) Recovering ground station liaison after/while stabilizing the target. If the position onto the target of the spacecraft is the top or rear of the stage, it may put the both of them into stabilizing spin along the axis of revolution of the target.

7. Decelerating thrust to get on a correct re-entry path.

8. controlled re-entry.

1.2 Space robotics' problem

There is one major problem for robotics in orbit: there is no fixed base. The problem is depicted on the schematic fig 7. This figure shows the trivial example of a 1-DOF space robot, trying to reach a goal depicted by the light circle on its right. On Earth, the manipulator would reach it by a 90° joint command, however in space there is no force compensating the reaction of the base. In this one problem, there are two issues: first, the end-effector did not reach the

[1]source: Chistophe Bonnal, chef de projets senior, Direction des Lanceurs du CNES

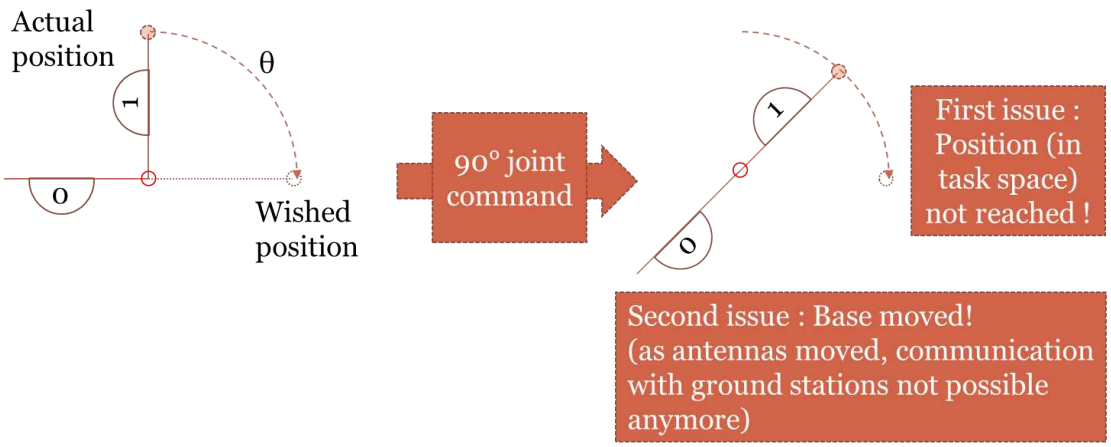

Figure 7: 1 DOF robot in space: simple depict of the problem, both link have the same inertia.

desired position, second, the base moved and the user is no longer able to communicate with the robot-satellite.

Of course this problem is not new and robotic systems have been used in space for a few decades now. However in most systems the base was way much more massive than the manipulated object (even in the Shuttle (RMS)), furthermore the base is often controlled through thrusters to keep the attitude of the base, emulating *de facto* a ground-based manipulator. When the base of the manipulator is not controlled, the satellite is said to be in free-flying.

1.3 Problem addressed

In a previous work, we implemented a GJM-based real-time control algorithm, suited for free-flying mode end-effector control. However, we would like to test it on the ground before implementing it on an actual satellite's arm. Even more so, we want to study what will happen when the satellite grab the two to three times more massive debris in Ariane 4's upper stage case (whereas in the Ariane 5 cryogenic stage case, the debris will be up to 7 times the first loop design mass of the chaser). The reader should refer to [10] for the estimated masses of the Ariane 4 targets, and [11] for the first loop design parameters of the chaser.

There are few works in the state of the art on this particular topic. Robotic missions in free-flying mode is quite new, so the facilities are not adapted for the tests of such missions. Traditionally, the facilities are either neutral buoyancy satellite in a huge pool, parabolic flights or "drop towers", offering a few seconds of weightlessness. Examples of such drop towers are the 145-meter drop tower facility at NASA's Glenn Research Center, Cleveland, Ohio, USA and the 146-meter ESA's ZARM drop tower at Bremen, Germany. Those towers offer respectively 5.2 seconds and 4.74 seconds of microgravity. The duration of the experiments are thus very short, the space very limited and the deceleration at the bottom of the shaft very high (up to 50G in ESA's ZARM case). Neutral buoyancy is not good either in the robotic tests because of the cost and the high friction coefficient due to the water.

Accordingly, the goal of this project is to design a mobile deck that allows a serial ma-

nipulator arm to react as it would in space, meaning the reaction of the base should not be compensated by the Earth's inertia as it would if the manipulator were fixed to the ground, confronted to:

- trajectories in world frame, or rather reaching of a target position specified in the world frame;
- the grasping of a massive object.

Two sub-goals are omnipresent: minimize the cost and volume occupied.

2 Preamble

There are two families of architectures to reach the first goal:

- 'Hardware in the loop' : instead of having an actual free base, the whole space manipulator is mounted on a serial robot which will move accordingly to the computed motion that the base would do if free-floating. The serial robot/deck for the mock-up can also be used in open-loop torque control to lift the weight of the mock-up robot in a so called "gravity compensation" mode, but the actuation of the joints leads to a very high equivalent friction coefficient. For an example of this architecture, refer to the European Proximity Operation Simulator (EPOS) facility at the DLR German Space Operations Center (GSOC) shown in [12] and on figure 8.
- Passive emulation of the free-floating environment : having the base of the space manipulator mounted on a device that allows up to 6 degrees of freedom to the robot, while being centred on the center of mass of it. For an example of this architecture, refer to the Free Flying Testbed (FFT) facility at the DLR Institute of Space Systems shown in [13] and on figure 9.

In light of the second goal, the second architecture is selected. However, we intend to put a robotic manipulator on top of the mobiles (Attitude Platform, AP), which leads to two main differences:

- the center of mass of the system, without any mass adjustments on the base or the robot or the payload (grabbing system) should be kept at the center of rotation of the AP;
- the scale will be much larger.

The different families of architectures are summed up in the following table 1 in the labels, while technological solutions are proposed. GSOC's EPOS facility corresponds to the active joints, deported rotation center solution while DLR's FFT facility correspond to the passive joints, not deported rotation center solution.

The goals-aimed-at lead to a passive joints solution, while the case considered, an emulation of a satellite+manipulator, imposes a deported rotation center solution.

The mobile deck will be composed of the three following platforms, shown on the figure 10:

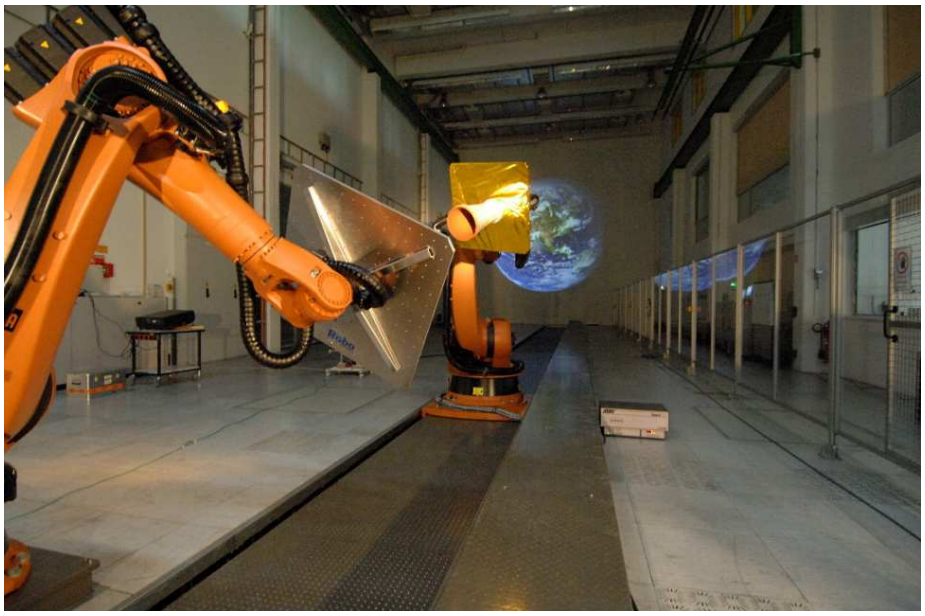

Figure 8: GSOC's EPOS facility: on the foreground a serial manipulator on which is fixed the base of the space manipulator, emulating the free-floating characteristic; on the middle ground a second serial manipulator, emulating the target; and in the background a picture of the Earth as seen by the chaser's vision system.

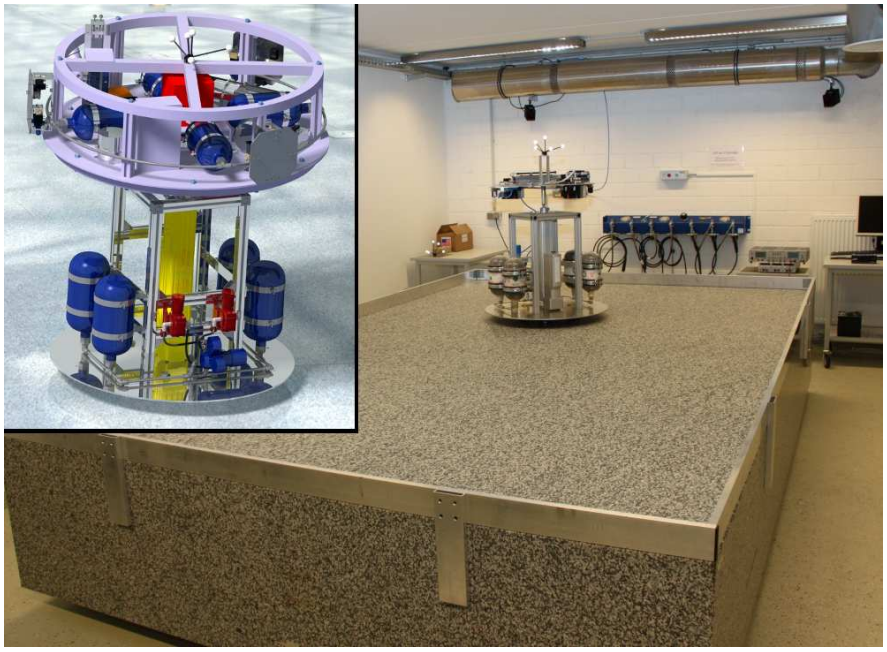

Figure 9: DLR's FFT facility: state of the facility as of august 2010, a huge marble plane, with a flatness below $3\,\mu m$, hosting a floating mobile called Transport Plateform (TP) depicted on the left side. These mobiles hover over the table, and host on a spherical air cushion another mobile called Attitude Platform (AP) hosting the mock-up of the satellite.

	Active joints	Passive joints (or back-drivable, for vertical axis)
Conventional joint (not deported rotation center)	6-pistons architecture	Shallow portion of a sphere on top of a fixed sphere +3 DoFs of translation
Deported rotation center	-Serial robot, $DoF \geq 6$ -Stewart platform	Circular cradles gyroscope +3 DoFs of translation

Table 1: Considered technological solutions depending on the controllability of joints and accessibility of the center of rotation.

- Transport Platform (TP): two degrees of freedom in translation perpendicular to the direction of gravity, and one active collinear with the gravity for position of the robot (to be understood: the center of mass of the robot, hence the center of rotation of the Attitude Platform, thanks to the Positioning Platform);
- Attitude Platform (AP): three degrees of freedom in rotation for attitude of the base;
- Positioning Platform (PP): three active degrees of translation to keep the center of mass of the mock-up of the space chaser at the center of rotation of the AP. (See section 5.2)

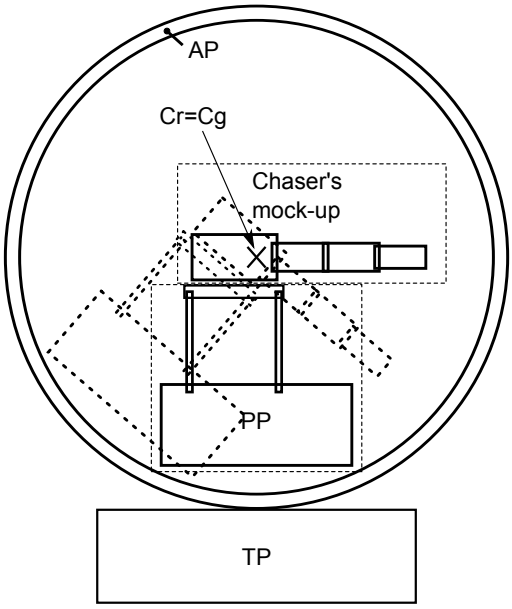

Figure 10: Schematic of the three platforms, along with the mock-up chaser.

3 Transport Platform

3.1 Architecture

As we consider the case of a reachable target, thus without any needs for translation actuators, the linear momentum should remain constant and thus this platform would not be needed. However the two goals aimed at impose the possibility of translations: in reality there might be induced external forces, and the contact with the object will definitively induce a translation as a counter-reaction. Moreover, due to the architecture of the rest of the test-bed (*ie* AP, PP, mock-up), the addition of cold gas thrusters is possible. In this case, the courses planned have to be added to the ranges of the translations.

The TP will be composed of 3 DoFs:

- two perpendicular passive DoFs for the motions perpendicular to the direction of the gravity;
- one DoF with a force-controlled actuator collinear with the gravity. The force-consign of this actuator is the weight of the AP, PP and space robot mock-up. The elements may be weighed separately to reach the necessary accuracy.

Without model of the contact phenomena, no ranges can be established. For this reason and also because of the duration of the project, the prototype will not include this platform but will be placed on a vibrant- or air-table, which will give the knowledge of the ranges needed for the future TP.

4 Attitude Platform

4.1 Architecture

The adopted architecture for the AP is inspired from the "human gyroscopes" used mainly in theme parks, as the examples shown on figures 11, 12. The principle is three cradles with concurring axes. In the case of this version of a gyroscope, it is basically 3 concentric circles linked by rotational joints placed at 90° of each other. This is the euler angles principle, and with the robot placed at the center it could rotate around the three axis.

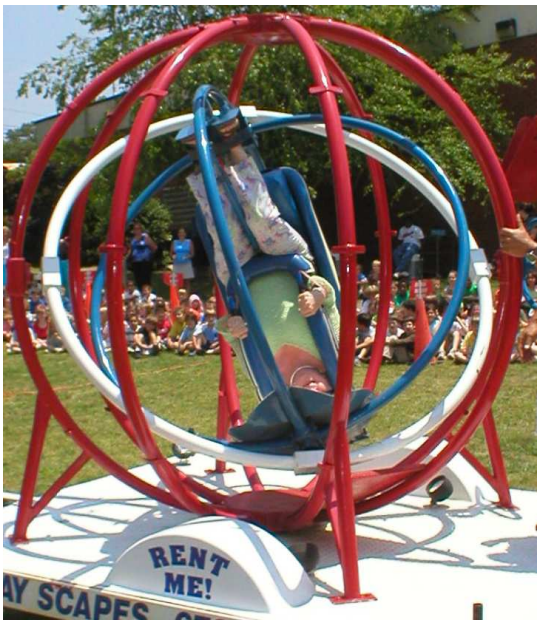

Figure 11: Human gyroscope for entertainment.

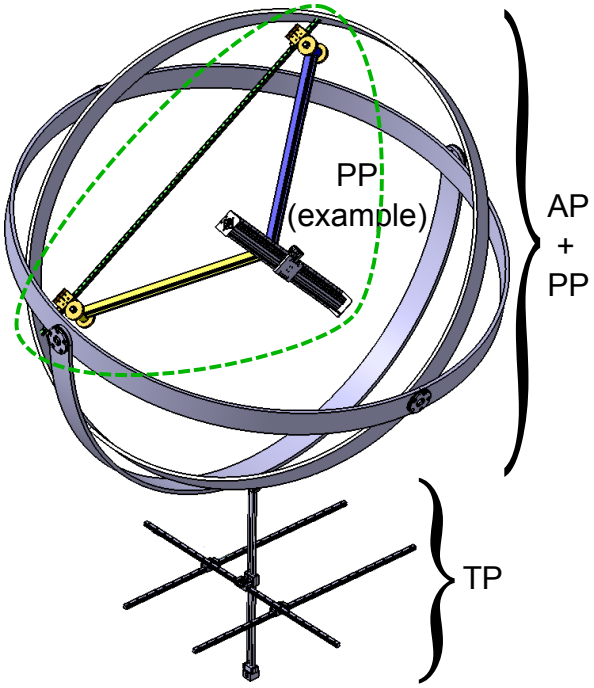

Figure 12: Circular cradles gyroscope. Architecture schematic depicting concepts for the three platforms.

However we want the robot to catch the target, and the sphere formed by those three circles in motion gets in the way of the target outside of the simulator. An answer is that it is possible to materialize the cradles by planar circular rails, among other solutions. This solution is privileged because it requires no power and seems cheaper than a portion of a sphere on gliders like on figure 13.

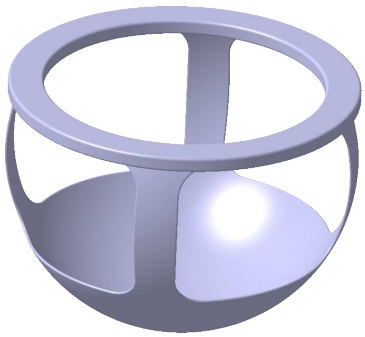

Figure 13: CAD model of a spheric AP, guided by several gliders beneath it to distribute the pressure.

The adopted solution consists of a hybrid between the cradle solution, using pivot links, and the circular rails solution, using circular translation links. The first link is a rotational joint with the axis collinear with the direction of gravity, linking the AP base to two perpendicular

circular rails. Out of this architecture several configurations for the last two DoFs are possible. There are two 1-DoF links to place amongst four sub-assemblies that are to be placed in a determined order, hence there is three combinatorial configurations. There is one additional configuration where the links can be merged in one 2-DoF link, inevitably between the inner and outer rails parts. Those four configurations are summed up in table 2.

DoFs	placement of CW	simplicity	comment
Base / Outer rails Outer / Inner rails Inner rails & PP	on: -outer rails -inner rails	+	$2 \times 1DoF$ case The CW to compensate the PP can be placed on the inner rails
Base / Outer rails Outer & Inner rails Inner rails / PP	on: -rails -PP's link	-	$2 \times 1DoF$ case Counterweights on the link with the PP
Base & Outer rails Outer / Inner rails Inner rails / PP	on: -inner rails -PP's link	-	$2 \times 1DoF$ case Counterweights on the link with the PP
Base & Outer rails Outer / Inner rails Inner rails & PP	on: -inner rails -rails' link	∘	$2DoF$ case All complexity reported on the 2 DoF part, CW on inner rails
The symbol / represents a rail/glider link, the symbol & represents a rigid link.			

Table 2: Possible configurations for the selected architecture. CW stand for counterweights. Those configurations of the two circular rails create only two rotational DoFs; the third is the rotation of the AP base.

As said earlier in the preamble, section 2, actuation defeats the second goal, of contact dynamics emulation: in the following, the possibility of actuation, either in the gliders or in the counterweights introduced later, is discarded.

We assume the PP is designed in such a manner that its center of mass is fixed in its basic reference frame, the one to be linked to the inner rails part. In order to emulate a momentum-free environment, the center of gravity of each "rigid assemblies", assemblies of parts without motion with respect to each of the other parts in the assembly, should coincide with the center of rotation of the AP. To do so, each so called rigid assembly is equipped with counterweights. See section 4.3 for the placement of those counterweights for the adopted solution. In order to counterbalance the mass of the rigid assembly considered, each counterweight has to be placed on the other side of the center of rotation, in reference of the rigid assembly considered. This necessity leads to long parts which need to be very rigid. This later constraint induce an increase of the mass of the part, hence in the mass of the counterweight, and so on.

This constraint considered, the first criterion of choice between those three configurations, in order to minimize the cost, is the number of counterweights, that is to be minimized. The second criterion of choice is the placement of the counterweights. The counterweights induce large parts circling around the mock-up chaser. Thus the closest rigid assembly equipped with counterweights to the mock-up chaser has to be empty of a hole of a radius of the length of the mock-up chaser to avoid collisions. See schematic 14 for a clearer explanation: it represents the four sub-assemblies in one plane, each link and rail equipped with hypothetical

counterweights, and the sphere of action of the mock-up chaser. Intersection with this later sphere would represents a possibility of collision.

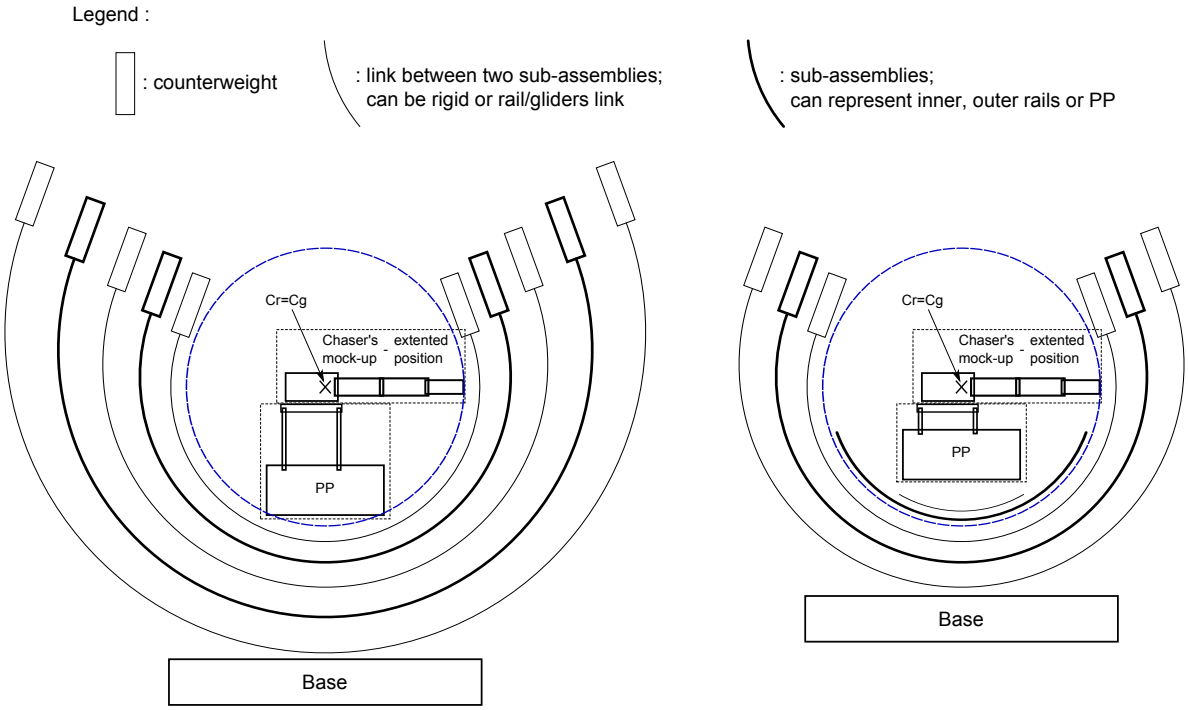

Figure 14: Schematic explaining the compactness criterion: on the left, there are counterweights on the very first link from the mock-up chaser, between the PP and the inner rails part; whereas on the right, the same link, without counterweights, can be integrated to the PP sub-assembly. On the same sub-figure is represented the inner rails part without counterweights which can then be integrated inside the sphere of action of the mock-up, at the price of some workspace.

The criterion is then: the farther the counterweights are from the mock-up chaser (or equivalently, of the center of the AP), the more compact the AP will be.

The adopted configuration, the 2 DoFs link (see schematic figure 15), is selected based on those two criteria.

4.2 Geometry of the inter-rails gliders

Due to the architecture selected, all the geometrical constraints have been reported to the part linking the two circular rails. The term glider alone is used for the assembly of the inner glider, the outer glider, and the linking part in-between: refer to figure 16. The two inner and outer gliders are sold by the manufacturer of the circular rails (specialized manufacturer: ROLLON *S.r.l.*, international linear motion systems manufacturer, headquarters in Italy. See also [14] for their curvilinear rails catalog). Those two gliders are sub-assemblies of a first part composed of a base plate with two axis around which wheel bases can pivot, two wheel bases composed of a stick and two wheel axis on the extremities, and four wheels placed on the two

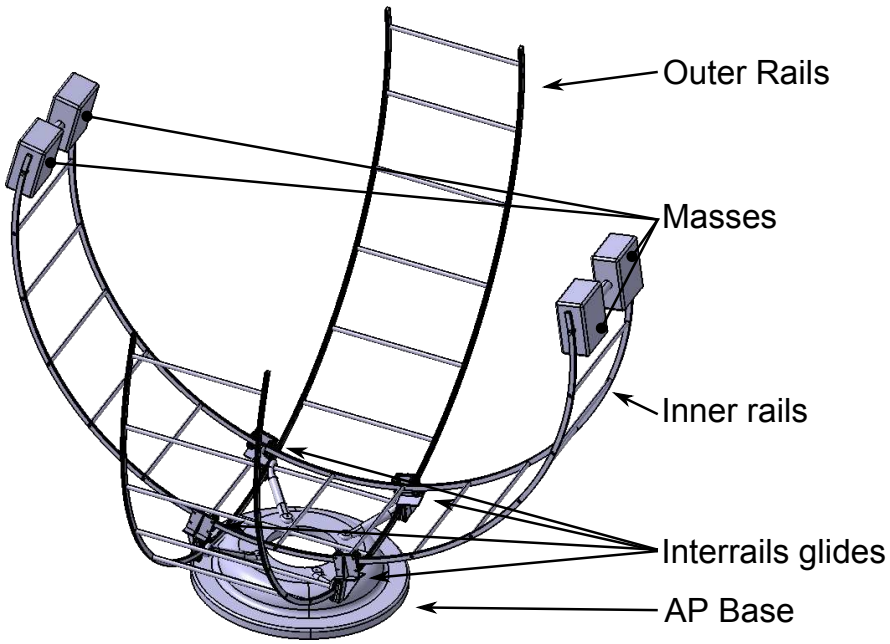

Figure 15: 2D gyroscope realized with rails. The third rotation is the rotation in the plane of the base. The counterweights on the glider parts are not depicted for clarity.

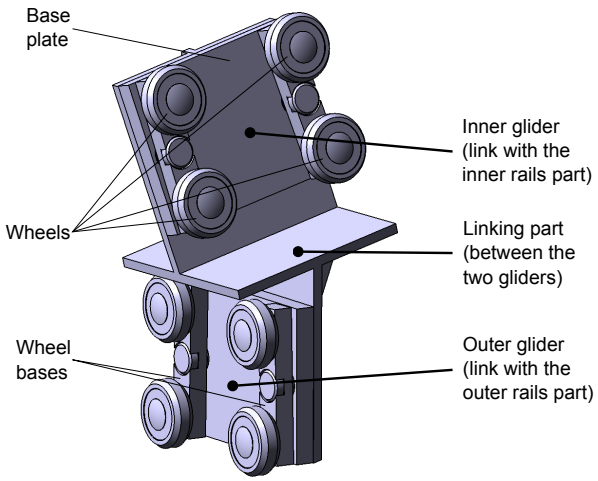

Figure 16: Glider, right-sided version.

wheel axis of the two wheel bases. The third part of the assembly is the part linking those inner and outer gliders sub-assemblies.

For the following explanations, please refer to the two schematics in appendix A, pages 31 and 32. The first one describes the geometry used: distances, points and the two main angles constrained by the AP assembly, while the second describes the frames and design angles used on the link part.

The two planes Ⓐ Ⓑ docking the inner and outer gliders are defined by 3 angles. The

definition of those three angles requires the complete geometrical definition of the AP. This geometrical definition is given in appendix A, page 31.

The point D is defined as the center of the middle plate of the link part. In the following, characteristic distances are defined, then angles with their derivation from the distances and geometrical relations.

4.2.1 Geometrical definition: Distances definition

On a first hand are presented the distances for the glider assembly (the importance of referring to the appendix page 31 for those definitions can not be stressed enough):

- e_{patin}, the serif between the axis of the two wheel bases;
- $pcca$, the distance between the center of the middle plate of the link, D, and the center of the inner glider (fasten on the plane Ⓐ); or equivalently, between D and the center of the outer glider (fasten on the plane Ⓑ);
- epf, distance between the two operating planes of the first part of the inner or outer gliders, namely the plane in contact with the operating planes of the link, Ⓐ or Ⓑ, and the plane in contact with the wheel base;
- pcr, the distance between this later plane but on the wheel base, and the base/working plane of the rail, equivalently the base/working plane of the wheels, equivalently the base/working plane of the wheel bases.

Related characteristic distances are defined for the rest of the global assembly of the AP:

- R_{int}, the radius of the base/working circle of the two inner rails;
- R_{ext}, the radius of the base/working circle of the two outer rails;
- c_{int}, the minimal distance between the center of the inner glider and the base/working circle of the inner rail, see figure 17:

$$c_{int} = R_{int} - \sqrt{R_{int}^2 - \left(\frac{e_{patin}}{2}\right)^2} \tag{1}$$

- c_{ext}, the minimal distance between the center of the outer glider and the base/working circle of the outer rail, see figure 17:

$$c_{ext} = R_{ext} - \sqrt{R_{ext}^2 - \left(\frac{e_{patin}}{2}\right)^2} \tag{2}$$

- a, the distance between two identical rails (the two inner rails or the two outer rails); this distance is a function of the momentum created by the application of the weight on the center of mass of the system, distant to the rails.

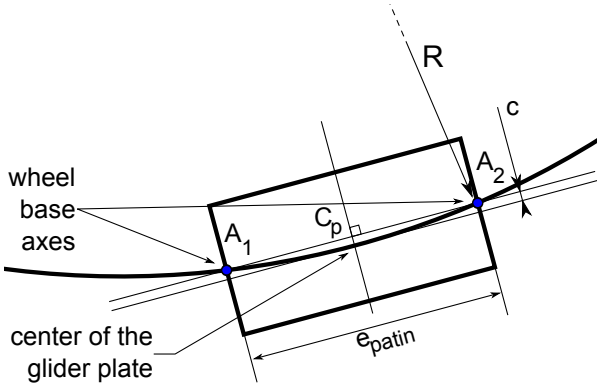

Figure 17: Schematic for the derivation of c_{int} and c_{ext}. R and c should be replaced by either R_{int} and c_{int} or R_{ext} and c_{ext}.

Moreover, as ED can be expressed in both planes of the figures page 31, the size of the link part can be expressed as a function of the radii of the rails, equation 3.

$$\text{on the left: } ED^2 = (R_{ext} - c_{ext} - pcca)^2 - \left(\frac{a}{2} + epf + pcr\right)^2$$

$$\text{on the right: } ED^2 = (R_{int} - c_{int} + pcca)^2 - \left(\frac{a}{2} + epf + pcr\right)^2$$

$$pcca = \frac{\sqrt{R_{ext}^2 - \left(\frac{e_{patin}}{2}\right)^2} - \sqrt{R_{int}^2 - \left(\frac{e_{patin}}{2}\right)^2}}{2} \tag{3}$$

Finally, the distance in-between two rails of the same part, a, depends on the torque applied on the part. The two parts are different cases:

- inner rails part: the weights of the inner rails part, including counterweights, the PP and the mock-up chaser applied at the center of rotation of the AP, create a torque on the outer rails part when the inner part is not vertical. The worst case is for the inner rails at a horizontal station, as depicted on figure 20. On top of that gravity-induced torque, there are the torques created by the actuators of the mock-up robot and of the PP. As the PP should be dynamically neutral to not induce parasitic motion, we assume its reaction torque to be nil. As of the mock-up robot, the worst case scenario is the maximum torque that can be applied on an actuator, available in the hardware specifications of the robot.
- outer rails part: the weights of the inner rails part and the PP are always applied at the center of rotation, thus inducing no torque on the always vertical outer rails, though the mock-up robot's center of mass can be slightly and temporarily out of the center of rotation of the AP. The torques created by the actuators of the mock-up robot are thus the main concern.

The ROLLON gliders can support stress in two directions and no momentum. See figure 18 and the table 19 for the directions and the maximum values of stress for the two kind of gliders available.

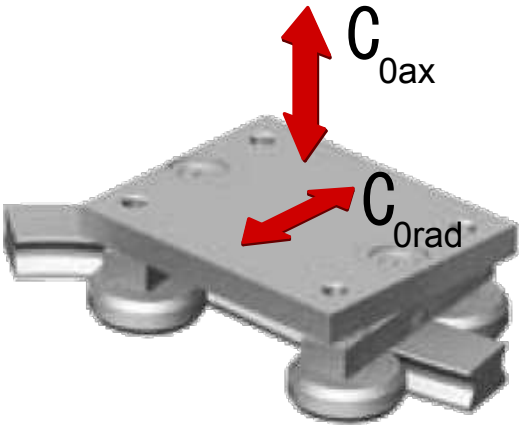

Figure 18: Directions of stress possible for both ROLLON's models of curvilinear gliders.

Glider Model	C_{0ax} [N]	C_{0rad} [N]
CCT08	400	570
CCT11	1130	1615

Figure 19: Values of the maximum payload, depending on the direction, allowed for each of the two models of glider for curvilinear rails in ROLLON catalog.

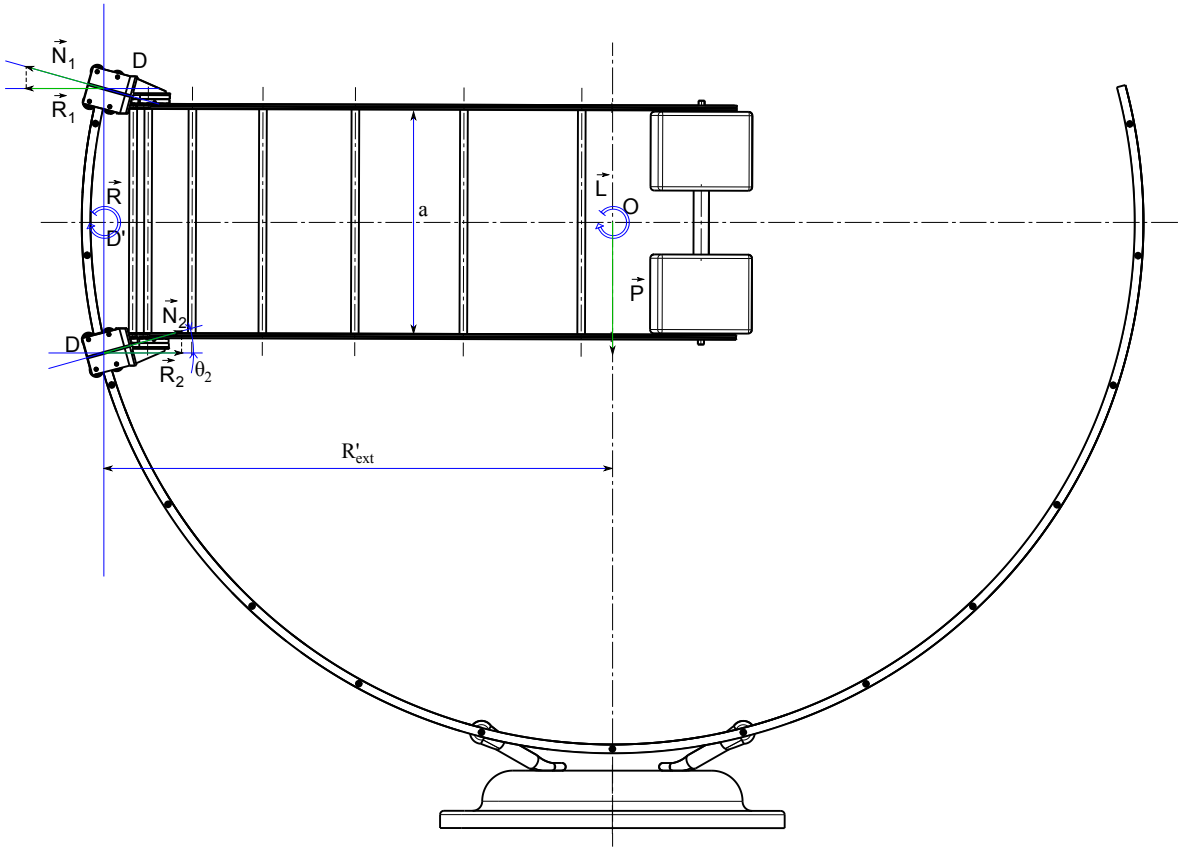

Figure 20: Derivation figure for the maximum momentum applied on the inner rails part.

Please refer to the figure 20 for the definition of the variables used in the following. The weight $\vec{P}$ of the inner rails part, PP and mock-up chaser, in addition of the torque $\vec{L}$ of the

actuators of the mock-up, creates the torque $\vec{R}$ given in equation 4. However this torque $\vec{R}$ can also be expressed as a function of the stress applied equally on the gliders, $\vec{N_1}$, $\vec{N_2}$, $\vec{N_3}$ and $\vec{N_4}$, in equation 5.

$$||\vec{R}|| = ||\vec{L}|| + ||\vec{P}||.R'_{ext} \tag{4}$$

$$||\vec{R}|| = 2 \cdot a \cdot ||\vec{R_1}|| = 2 \cdot a \cdot \sqrt{1 - \frac{a^2}{4 \cdot R_{ext}^2}} \cdot ||\vec{N_1}|| = 2 \cdot a \cdot \frac{R'_{ext}}{R_{ext}} \cdot ||\vec{N_1}|| \tag{5}$$

Assuming, as this is the worst momentum loading, that the gliders are at their maximum capacity, then $||\vec{N_i}|| = C_{0rad}$. Hence the derivation of the value a in equation 6, or considering that $\vec{L}$ is negligible in front of the huge weight at the end of the big cantilever in equation 7.

$$a = \frac{||\vec{L}|| \cdot \frac{R_{ext}}{R'_{ext}} + ||\vec{P}||.R_{ext}}{2 \cdot C_{0rad}} \tag{6}$$

$$a \approx \frac{||\vec{P}||.R_{ext}}{2 \cdot C_{0rad}} \tag{7}$$

Considering the mock-up composed of the KUKA LightWeight Robot, its maximum payload, a base about three times the payload, and the PP lighter than $20\,kg$, then the first loop design value of a is below $700\,mm$.

4.2.2 Geometrical definition of angles and derivation

The middle plate of the link part is defined by the directions of the tangent to the inner rail and the tangent to the outer rail, and serve as a base for this part. The frame $\mathcal{R} = (\underline{x}, \underline{y}, \underline{z})$ is assigned to it using those directions and attached at the point D, the center of the middle plate, $\underline{y}$ being perpendicular to the plate.

The intersection of the plane parallel to the inner rail plane through D with the axis of the inner rails is called O'. The intersection of the plane parallel to the outer rail plane through D with the axis of the outer rails is called O". The projection of O' on the plane parallel to the outer rail plane through D, or equivalently the projection of O" on the plane parallel to the inner rail plane through D, is called E. The correspondence of those two projections does not depend on whether the distance a is identical for both pairs of rails, but on the perpendicularity of the inner and outer rails parts.

The inner plane, Ⓐ, is directed by the tangent to the inner rails and the segment perpendicular to the axis of the inner rails part through D. This later segment is also defined by the angle α to the radius of the outer rail through D in the plane parallel to the outer rail plane through D. Considering the right triangle $O"ED$ comes the derivation of α, equation 8.

$O"E = \frac{a}{2} + epf + pcr$, and $O"D = R_{ext} - c_{ext} - pcca = \sqrt{R_{ext}^2 - \left(\frac{e_{patin}}{2}\right)^2} - pcca$, thus:

$$\alpha = \arcsin\left(\frac{\frac{a}{2} + epf + pcr}{\sqrt{R_{ext}^2 - \left(\frac{e_{patin}}{2}\right)^2} - pcca}\right) \tag{8}$$

In a similar manner, the outer plane, Ⓑ, is directed by the tangent to the outer rails and the segment perpendicular to the axis of the outer rails part through D, which is also defined by the angle β between the outer plane Ⓑ and the radius of the inner rail through D in the plane parallel to the inner rail plane through D. Considering the right triangle $O'ED$ comes the derivation of β, equation 9.

$$O'E = \frac{a}{2} + epf + pcr, \text{ and } O'D = R_{int} - c_{int} + pcca = \sqrt{R_{int}^2 - \left(\frac{e_{patin}}{2}\right)^2} + pcca, \text{ thus:}$$

$$\beta = \arcsin\left(\frac{\frac{a}{2} + epf + pcr}{\sqrt{R_{int}^2 - \left(\frac{e_{patin}}{2}\right)^2} + pcca}\right) \tag{9}$$

The third angle is the perpendicularity between the two planes.

4.2.3 Design angles and derivation

The previous angles are the specification angles. The design angles of the part, which have to satisfy the specification angles, are noted with the index 0. The point of those design angles is that the geometrical definition of the part stands alone of the assembly. Moreover, the rotation of the base frame around the tangent to the outer rail induce a rotation of the plane Ⓐ, or the other way around as Ⓐ and Ⓑ are defined relatively to each other. The specification α is thus not defined in a physical plane on the part, and an angle γ_0 around the normal to the middle plane is introduced to get the perpendicularity between the inner and outer planes Ⓐ and Ⓑ.

A set of reference frames are defined on the link part, see page 32. The frame $\mathcal{R}_1 = (\underline{x_1}, \underline{y_1}, \underline{z_1})$ is attached to the plane Ⓐ, while the frame $\mathcal{R}_3 = (\underline{x_3}, \underline{y_3}, \underline{z_3})$ is attached to the plane Ⓑ. There is also a transitional frame $\mathcal{R}_2$ defined. The common origin of the four frames is D.

As the planes are defined relatively to each other, either α_0 or β_0 has to be set to its specification. $\beta_0 = \beta$ is chosen, leaving α_0 and γ_0 to be derived.

Expressed with the frames, the perpendicular condition between Ⓐ and Ⓑ is equivalently expressed by the equations 10.

$$y_3 z_3 \perp x_1 y_1 \Leftrightarrow x_3 \perp z_1 \Leftrightarrow x_3.z_1 = 0 \tag{10}$$

Now, the projection of x_3 in $\mathcal{R}_1$ is given equation 11.

$$x_3.z_1 = -\sin(\beta_0) \cdot \sin(\alpha_0) + \cos(\beta_0) \cdot \sin(\gamma_0) \cdot \cos(\alpha_0) \tag{11}$$

Equations 10 and 11 give γ_0, equation 12.

$$\sin\gamma_0 = \tan(\beta_0) \cdot \tan(\alpha_0) \tag{12}$$

The specification α end up being the angle between the planes Ⓐ and the plane perpendicular to Ⓑ, x_3y_3: $\alpha = (\widehat{x_3y_3; x_1y_1})$, or equivalently between the normal vectors to those

planes, $\alpha = \widehat{(z_3; z_1)}$. Hence we can express the projection of z_3 on z_1 with α, equation 13, or through the construction angles, equation 14.

$$z_3.z_1 = \cos\alpha \tag{13}$$

$$z_3.z_1 = \cos(\alpha_0) \cdot \cos(\gamma_0) \tag{14}$$

Using few trigonometric relations, the design angle α_0 is expressed as a function of the characteristic distances and the angle β_0, equation 15. *need/usefulness of the derivation? TBM*

$$\alpha_0 = \arcsin\left(\frac{\frac{a}{2} + epf + pcr}{\sqrt{R_{ext}^2 - \left(\frac{e_{patin}}{2}\right)^2} - pcca}\cos(\beta_0)\right) \tag{15}$$

This derived geometry will not be met in reality, as it would need perfect angles that even the CAD software tool have a though time to meet. However, the bores in the glider's link allow some play before fastening the gliders on. Thereby, the assembly of the gliders will be done without tightening at first, mounted on both rails and then tightened while motioning the system to make sure the assembly is not working for only one position.

4.3 Kinetics of the AP

Please refer to the schematic figure 15. The frame used is as follow: the $\underline{y}$-axis is perpendicular to the plane of the base and corresponds to the direction of the acceleration of gravity, and in the initial configuration depicted on the schematic, the $\underline{z}$-axis is the axis of the outer rails and the $\underline{x}$-axis is the axis of the inner rails.

4.3.1 Inner rails part

As the inner rails part rotates around all three axes, its center of mass, or center of gravity, C_g (with the hypothesis of uniform gravitational field) must coincides with the center of rotation C_r of the AP. To do so, the angular sector of this part must be over half a circle. The inner rails are equipped with counterweights to compensate for their own weight and of the PP. The weight of mock-up chaser (hence including base, manipulator and payload) is not compensated as its center of mass is already at the center of rotation of the AP, thanks to the PP. The wider the angular sector is, the lighter the counterweights are. This converges back to the circular cradles gyroscope solution. A middle ground was selected, see schematic figure 15.

4.3.2 Inter-rails gliders

Those four gliders perform rotational translations around two axis: perpendicular to the plane of the base and around the axis of the outer rails part. The intersection of those two axis is once again the center of rotation of the AP. To send the center of gravity of the gliders at the center of rotation, the same solution than of the inner rails part is adopted: an angular sector equipped with a counterweight deports the center of mass. Those counterweight parts are not depicted on the schematic figure 15 in order to keep the clarity of it, but they are shown on

the AP prototype figures, see section 6. Even if the four gliders are independents, they act as if linked, due to the architecture. Hence, each have a counterweight addition deporting their center of mass in a plane parallel to the plane of the base and containing the center of rotation. The barycenter of the four gliders then coincides with the center of rotation of the AP.

4.3.3 Outer rails part

This part rotates around one axis, perpendicular to the plane of the base. Hence, its center of gravity should be on this axis, which is the case by construction. For this part, no need for counterweights, nor constraints on the angular sector. However, the center of gravity of the outer rails and the base should be aligned on an axis perpendicular to the plane of the base: the only constraints are alignments constraints between the outer rails part and the base.

4.4 Dynamics at the center of rotation: study of the equilibrium and stability

In space and in weightlessness state, there are no other forces beside from the robotic satellite. Statically, this induces that the attitude of a body will not change if no torque is applied on it. Dynamically, it induces that when a torque produces an acceleration of a body, the motion will not stop until there is an adequate torque applied in the opposite direction.

In order to statically emulate this behaviour, the center of mass of each sub-assembly has to coincide with the center of rotation - see previous section 4.3. High friction in the links could help to compensate for the unavoidable gap between the centers of mass and the center of rotation, but it would really hinder the dynamical emulation, so it is discarded. Instead, beside the fixed masses on each sub-assembly, room is left to add small washers on the counterweights links (medium tune of the CW) and magnets on the ferromagnetic counterweights (fine tune).

In order to dynamically emulate this behaviour in the AP, not only the friction in the links has to be minimized but the mass distribution within the parts has to induce an equilibrium behaviour for all positions within the ranges. The mass distribution within a sub-assembly is characterised by its inertia matrix.

The dynamical behaviour expected can be traduced as an absence of variations in the kinetic energy function for no command torque applied, assuming a perfect absence of friction.

In this section, the kinetic energy function is derived in order to work out the specifications on the mass distribution in the three cases of motion (rotation around one, two or three axes that the outer rails part, the four gliders and the inner rails part respectively describe).

The kinetic energy function is half of the co-product of the twist screw and the momentum screw. Equations 16 and 17 represent respectively those two screws given at P point in frame R for any solid S in motion.

$$\{\mathcal{V}_{S/R}\}_P = \left\{ \begin{array}{c} \overrightarrow{\Omega_{S/R}} \\ \overrightarrow{V^P_{/R}} \end{array} \right\} \tag{16}$$

$$\{\mathcal{C}_{S/R}\}_P = \left\{ \begin{array}{c} m_S \cdot \overrightarrow{V_{S/R}} \\ \overrightarrow{\sigma^P_{S/R}} \end{array} \right\} \tag{17}$$

At the center of mass G of the solid, the kinetic momentum is reduced to the product of the inertia matrix of the solid at the center of mass by the twist vector, equation 18.

$$\overrightarrow{\sigma^P_{S/R}} = \underline{\underline{J_G}}(S) \cdot \overrightarrow{\Omega_{S/R}} \tag{18}$$

Thus, the kinetic energy function of a sub-assembly Σ (with no internal motion) is given equation 19.

$$2 \cdot T = \{\mathcal{V}_{S/R}\}_G \otimes \{\mathcal{C}_{S/R}\}_G = m(\Sigma) \cdot \overrightarrow{V^G_{/R}}^2 + \overrightarrow{\Omega_{S/R}} \cdot \underline{\underline{J_G}}(S) \cdot \overrightarrow{\Omega_{S/R}} \tag{19}$$

The system is in an equilibrium state if and only if at the position $q = (\theta_3, \theta_1, \theta_2)$ the kinetic energy function has no variations, or equivalently if all partial derivatives of the kinetic energy are nil.

4.4.1 Analysis of the first term

In the frame of the base of the AP, the velocity of the center of rotation is nil. However, as said earlier, there is a gap between the center of rotation and the center of mass of the sub-assembly, as described by the equation 20. Because of this gap, for a rotational motion $\overrightarrow{\Omega_{\Sigma/R}} = \dot{\theta} \cdot \vec{a}$, the velocity of the center of mass is not exactly nil, equation 21.

$$\exists x \in \mathbb{R}^*, \vec{u} \in \mathbb{R}^3 - \{\vec{0}\} \quad \overrightarrow{C_g G} = x \cdot \vec{u} \tag{20}$$

$$||\overrightarrow{V^G_{/R}}|| = ||\overrightarrow{V^{C_r}_{/R}} + \overrightarrow{\Omega_{S/R}} \wedge \overrightarrow{C_g G}|| = x \cdot \dot{\theta} \cdot \sin\left(\widehat{\vec{a}, \vec{u}}\right) \tag{21}$$

Thus, in order to minimize the variation of the first term of the kinetic energy, $m(\Sigma) \cdot \overrightarrow{V^G_{/R}}^2$, the gap need to be minimized and the ranges/speed rates kept small (but the later interferes with requirements).

4.4.2 Analysis of the second term

At first, we consider complete inertia matrices in the sub-assembly frame $J(\Sigma_0)$ for every sub-assembly, such as equation 22. This means the inertia products are non-zero, although theoretically, the geometry of the three sub-assemblies presents 2 planes of symmetry due to the static emulation (correspondence C_G-G) leading to diagonal inertia matrices in the sub-assembly frame.

$$J_G(OR) = \begin{bmatrix} A0_{OR} & -F0_{OR} & -E0_{OR} \\ -F0_{OR} & B0_{OR} & -D0_{OR} \\ -E0_{OR} & -D0_{OR} & C0_{OR} \end{bmatrix} \tag{22}$$

Using an analytical solver (Maple), the inertia matrices $J(\Sigma)$ are derived in the AP base frame for any position $q = (\theta_3, \theta_1, \theta_2)$, followed by the kinetic energy term, equation 23, and its three

partial derivatives. The rotation rate matrices Ω_Y, Ω_Z, Ω_X are function of the angular speed on the eponymous axis, and do not depend on the position q.

$$\begin{aligned} T_2 = 1/2 \cdot \Big(& \Omega_Y . J\left(OR\right) . \Omega_Y \\ & + \left(\Omega_Y + \Omega_Z\right) . J\left(gliders\right) . \left(\Omega_Y + \Omega_Z\right) \\ & + \left(\Omega_Y + \Omega_Z + \Omega_X\right) . J\left(IR\right) . \left(\Omega_Y + \Omega_Z + \Omega_X\right) \Big) \end{aligned} \tag{23}$$

The results are that to nullify the variation, hence the partial derivatives, either the rotational speeds should be nil (back to static case emulation), either the inertia matrices $J_G\left(IR\right)$, $J_G\left(gliders\right)$, $J_G\left(OR\right)$ should be as in equation 24: diagonal for the sub-assemblies which rotate around two or three axes (gliders and inner-rails part) and for all sub-assemblies their three main inertiæ should be identical.

$$\begin{bmatrix} A0_{IR} & 0 & 0 \\ 0 & A0_{IR} & 0 \\ 0 & 0 & A0_{IR} \end{bmatrix}, \begin{bmatrix} A0_p & 0 & 0 \\ 0 & A0_p & 0 \\ 0 & 0 & A0_p \end{bmatrix}, \begin{bmatrix} A0_{OR} & -F0_{OR} & -E0_{OR} \\ -F0_{OR} & A0_{OR} & -D0_{OR} \\ -E0_{OR} & -D0_{OR} & A0_{OR} \end{bmatrix} \tag{24}$$

The definition of stability is that for a position q_s, with non-nil initial conditions in position and speed, the system goes back to q_s. This definition is equivalent to the strict negativity of every eigenvalues of the kinetic energy second derivatives matrix.

With such inertia matrices, the eigenvalues of the kinetic energy second derivatives matrix are nil (as the matrix is identically nil). This result is coherent with the goal: no stability in the strict meaning, as the system should not "go back" to any position, but instead a stability in the motion.

The equality of all the main inertiæ is characteristic of uniform spheres (empty or not). There are two possibilities to nullify the variation of the second term of the kinetic energy of the system:

- Once again, keep the ranges of variation/speed rates small (not really a solution as it interferes with the requirements);
- The addition of small masses on the sides of the parts, preferably at the end of cantilevers.

The solution of cantilever is rejected due to the problems it produces (bending load induced by the gravity, collisions, non-accessibility to the outside of the testbed). Even if the addition of masses on the sides is not ideal, as it greatly increases the masses of the parts, it is selected to reduce, not nullify, the variation of kinetic energy.

5 Positioning Platform

5.1 Architecture

The problem is that with a robot as a satellite, the center of mass is not at a constant position, but the center of rotation needs to be placed at the center of mass of the chaser's mock-up

when occurs a motion of the joints or when an external force or momentum is applied. Thus the goal is to keep the center of mass at the center of rotation at all times. The choice of the architecture is driven by two criteria specific to the application and two criteria inherent of embarked robots:

- conservation of the attitude of the end-effector in reference to the base of the PP;
- feasibility to add a subsystem to keep the center of mass of the PP constant in its base frame, or equivalently in the last frame of the AP;
- minimization of the mass of the PP, in order to minimize the mass of the counterweights;
- number of DoF; 3 translations are needed as well as the conservation of the attitude of the end-effector, potentially needing a 6-DoF robot.

Several architectures keeping the end-effector attitude were considered: Cartesian, achieving first two criteria; a hybrid between parallel and serial robot to satisfy the mass criterion which can be seen on the principle schematic figure 12; and finally a totally parallel architecture materialized as a rotational Delta robot, achieving all four criteria at the price of a more complex system and command.

5.2 Kinetics and simplified dynamics

In order to keep the center of mass of the platform at a fixed position within the inner AP frame, the Delta robot is backed up with his twin, but oriented towards the other side of the base of the Delta robot, and loaded with a mass equal to the chaser mock-up. The commands on this twin Delta are the same that on the main Delta; this way the center of mass of the PP is fixed with reference to the inner circular rail of the AP and the weight of the PP is compensated by fixed masses on the inner circular rail of the AP.

However the twin motion of those two Deltas generates momentum on the AP on two axis. This momentum will be compensated by two reaction wheels mounted on the base of the Delta robots.

5.3 Sizing of the Delta and positioning relatively to the inner rails part

Now that the solution of the 3-rotations Delta robot is selected, there are 3 parameters to derive from wished workspace, available space and non-collision considerations: length of forearms L_A, length of arms L_B, and position in the inner rails part, on the AP, characterised by H_f. To do so, the parameter θ_i is defined between the base and the i-th forearm, and allows to differentiate cases in the following. Those parameters are defined in situation on the schematic 21.

The desired workspace proposed is set as a sphere centred on the center of rotation of the AP. While sizing the robot, a sub-objective is to maximize this work-sphere. It will be a function of ϕ_{IR}, radius of the inner rails part.

The first parameter to be derived is the length of the arms L_B, as it depends only on the desired workspace. The later is a sphere that should fit inside the workspace of the Delta,

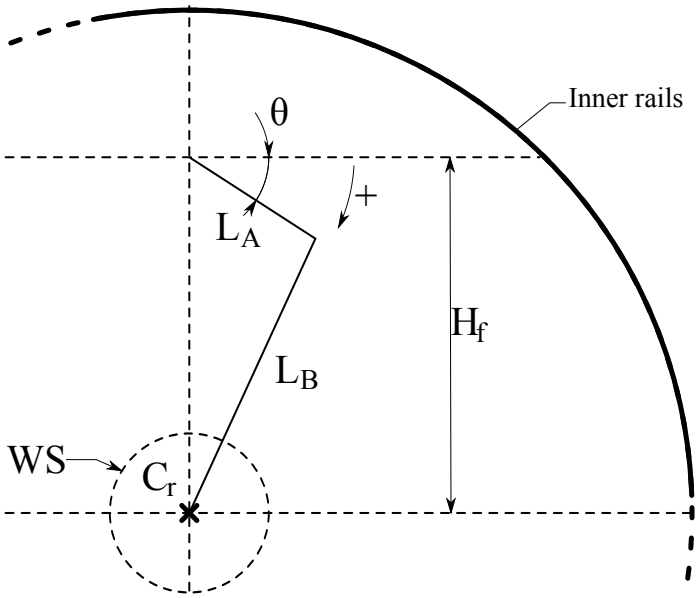

Figure 21: Derivation figure for the parameters conditioning the PP. WS stands for the desired WorkSpace. Only one of the three arms are depicted, but the L_A and L_B lengths are identical for the three arms.

which is faceted in a hexagonal cylinder with 1.3 times the length of the arms L_B between two opposed faces. Thus the length of the arm, equation 25.

$$L_B = \frac{\phi_{\mathrm{WS}_{\mathrm{desired}}}}{1.3} \tag{25}$$

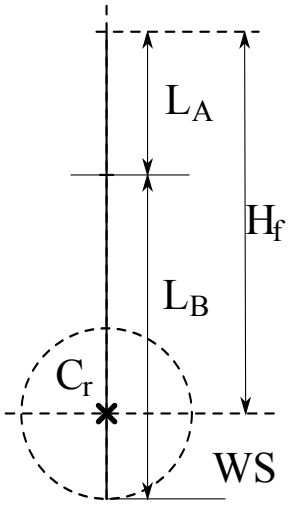

Figure 22: Extended Delta arm reaching the bottom of the desired workspace.

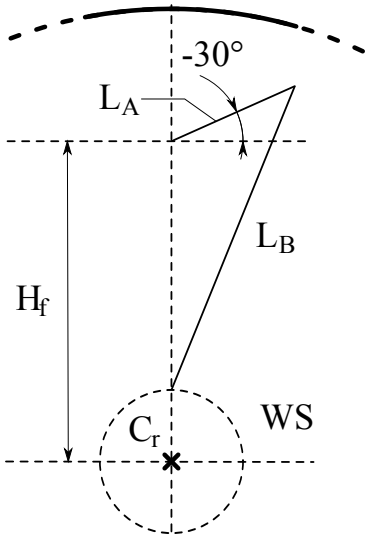

Figure 23: "Folded" (minimal extremum) Delta arm reaching the top of the desired workspace.

Second is the relation between the position of the Delta and the lengths of the forearm and arm. Considering that the end-effector needs to reach the bottom of the workspace, the command would hypothetically be $\theta_{ie1} = 90^{\circ}$, as pictured on figure 22. This gives a condition between those two lengths, equation 26.

$$L_A + L_B \geq H_f + \frac{\phi_{WS}}{2} \Leftrightarrow H_f \leq L_A + L_B - \frac{\phi_{WS}}{2} \tag{26}$$

However, in the other extremum position for the minimal value of the command angles, the arms should not interfere with the rest of the system, refer to the figure 23. The equation 27 translates this later condition. In order that the twin Delta does not hinder the mock-up motion, the lower limit proposed for the command angles is $\theta_{ie2} = -30^{\circ}$. In this position, the end-effector should also reaches the top of the workspace sphere, equation 28.

$$\forall \theta_i \in [\theta_{ie2}; \theta_{ie1}], \quad ||\overrightarrow{H_f} + \overrightarrow{L_A}|| \leq \frac{\phi_{IR}}{2} \tag{27}$$

$$\text{For } \theta_i = \theta_{ie2}, \quad ||\overrightarrow{L_A} + \overrightarrow{L_B}|| \leq H_f - \frac{\phi_{WS}}{2} \tag{28}$$

Using Al-Kashi relation and equation 26, equations 27 and 28 lead to quadratic equations, solved by the two inequalities 30 and 32 on L_A, associated with the two conditions 29 and 31, from the discriminants of the quadratic equations.

$$(2L_B - \phi_{WS})^2 \cdot (\sin\theta_{ie2} - 1) + 2 \cdot \phi_{IR}^2 \geq 0 \tag{29}$$

$$L_A \leq \frac{1}{4} \cdot \left(\sqrt{(2L_B - \phi_{WS})^2 - \frac{1}{2} \frac{(2L_B - \phi_{WS})^2 - \phi_{IR}^2}{1 + \sin\theta_{ie2}}} - (2L_B - \phi_{WS}) \right) \tag{30}$$

$$(L_B - \phi_{WS})^2 \cdot (\sin\theta_{ie2} - 1) + 2 \cdot L_B^2 \geq 0 \tag{31}$$

$$L_A \geq \frac{1}{2} \cdot \left(\sqrt{(L_B - \phi_{WS})^2 - 2 \cdot \frac{(L_B - \phi_{WS})^2 - {L_B}^2}{1 + \sin\theta_{ie2}}} - (L_B - \phi_{WS}) \right) \tag{32}$$

The equations 25, 30 and 32 give the derivations of the three parameters, L_A, L_B, H_f and the size of the workspace ϕ_{WS} allowed by the chosen robot and imposed conditions (in particular the values of extrema). Those derivations are equations 33 through 36.

$$L_B = \frac{1}{2} \cdot \sqrt{48\phi_{WS}^2 + (\phi_{WS} - \phi_{IR})^2} - 3 \cdot \phi_{WS} \tag{33}$$

$$L_A = -\frac{1}{4} \cdot \sqrt{48\phi_{WS}^2 + (\phi_{WS} - \phi_{IR})^2} + \frac{1}{4} \cdot \phi_{IR} + \frac{7}{4} \cdot \phi_{WS} \tag{34}$$

$$H_f = \frac{1}{4} \cdot \sqrt{48\phi_{WS}^2 + (\phi_{WS} - \phi_{IR})^2} + \frac{1}{4} \cdot \phi_{IR} - \frac{7}{4} \cdot \phi_{WS} \tag{35}$$

$$\phi_{WS} \leq 0.2518 \cdot \phi_{IR} \tag{36}$$

Equations 33 through 35 give the limits of the tolerance intervals for each parameters, for ϕ_{WS} from the proposed value through its maximal value, reached at the equality in equation 36.

The maximisation of the workspace minimises the interval of values for the three parameters. If there were no looseness in the links and the parts were perfect and inelastic, the workspace sphere could be as big as 25.18% of the radius of the inner part. Thus, the last criteria allowing the determination of the three parameters and the size of the workspace is the size of the intervals of values for the parameters.

For this criteria of the size of the intervals, 1% of the diameter of the inner part is proposed. This leads to a workspace diameter about 18.5% of the diameter of the inner part. In the case of a mock-up based on the KUKA's LWR, the size of the inner part would be $\phi_{IR} = 2.4\,m$, hence with the 1% criteria the tolerances width is about $24\,mm$ to compensate play in the links, process tolerances and elasticity of the parts; the workspace is a sphere of $0.444\,m$ in diameter.

On figure 24 is depicted the evolution of the width of the tolerances along of the size of the workspace. If the criteria were set up to 10% of the diameter of the inner part, the workspace would be reduced at a sphere of a diameter about 2.5% of the diameter of the inner part. Still in the KUKA's LWR case, those proportions represent tolerances width about $240\,mm$ and diameter workspace about $60\,mm$.

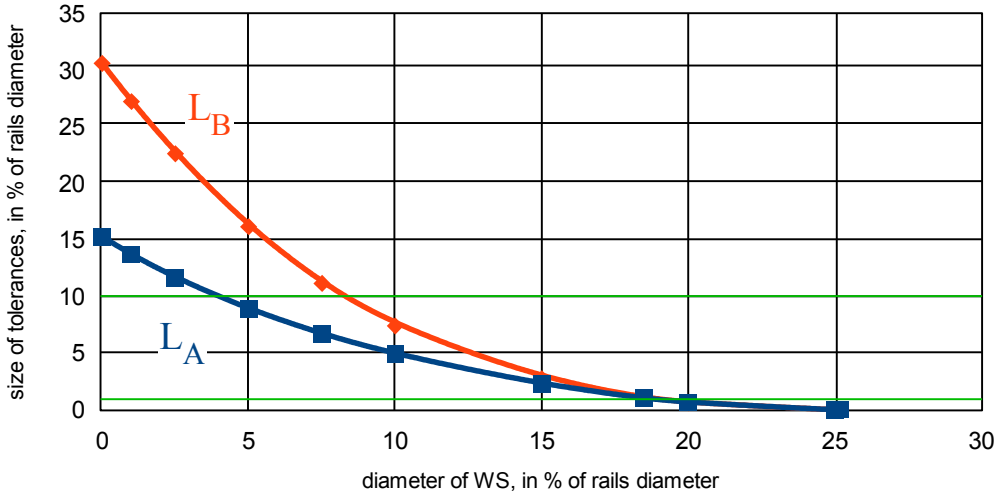

Figure 24: Widths of the tolerances versus size of the workspace.

6 Prototype of the AP

On figures 25, 26, and 27 are depicted the CAD model for the prototype of the AP in neutral position $q_0 = (0, 0)$, extreme position of the Z range $q_{Ze} = (38^\circ, 0)$, and extreme position of both Z and X ranges $q_{ZeXe} = (38^\circ, 45^\circ)$. In spite of blueprints submission on the 15th of December, the prototype is not yet ready to proceed to any test, hence the absence of test results.

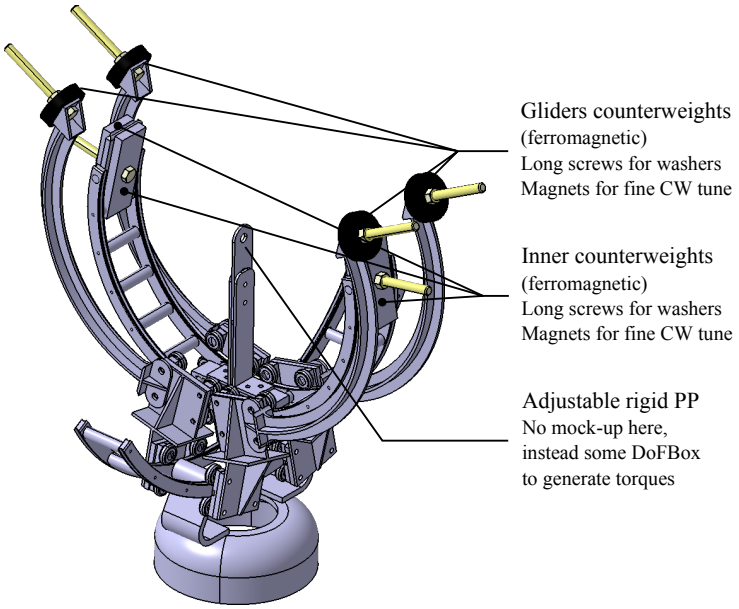

Figure 25: CAD model for the prototype of the AP in neutral position $q_0 = (0, 0)$. Screws (long yellow cylinders) are long to be able to add some washers (medium CW tune). Counterweights are ferromagnetic to add magnets for fine tune.

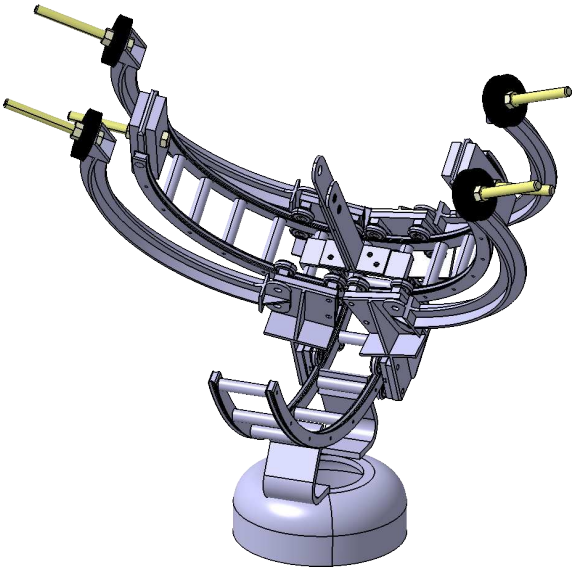

Figure 26: CAD model for the prototype of the AP in extreme position of the Z range $q_{Ze} = (38^\circ, 0)$.

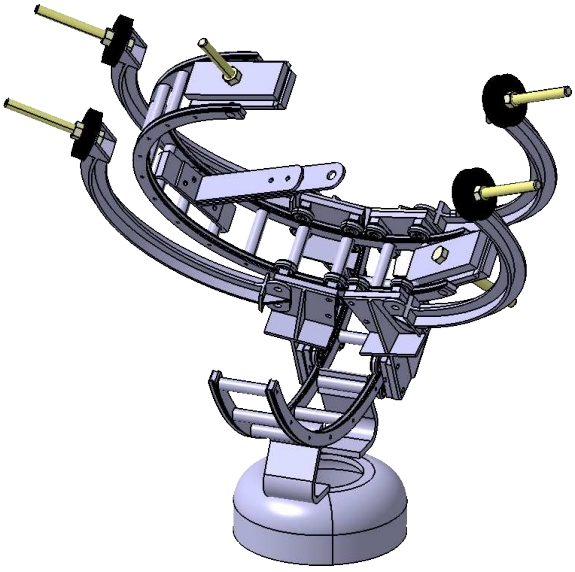

Figure 27: CAD model for the prototype of the AP in extreme position of both Z and X ranges $q_{ZeXe} = (38^\circ, 45^\circ)$.

However, even in the absence of prototype, the ROLLON circular guide have been order in another laboratory and the quality requirements are not met. The main problem is that the mobile encounters stiff positions at each bore in the guide. Another provider is considered,

THK [15], but their angular parts are up to 141°, inducing the necessity of a connexion between two parts to meet the angular sector needed for the inner rails which can be problematic.

Other solutions are considered, such as the portion of sphere solution brought up in section 4.1.

7 Conclusion

A good emulating deck is needed, especially for contact dynamics try-outs. However the presence of a robot on the satellite is bothersome as it makes the center of mass mobile. An active platform cannot achieve the force-free environment requirements, but a completely passive platform can not adapt for the displacement of the center of gravity. The rail-based gyroscope presented here is a mixture of both solutions: passive links for the reaction of the satellite to the motion of the robot, and an active platform to handle the mobility of the center of mass.

The theory shows that this design should work nicely, and a lot of defaults due to the transition from model to reality were thought-out. The most important is certainly the tuning of the masses of the counterweights and their distribution *via* the addition of washers (medium tune) and magnets (fine tune). However, the solution of rollers/guide, while cheap, may not be good enough to achieve the force-free requirements. An AP prototype is absolutely required to qualify the solution.

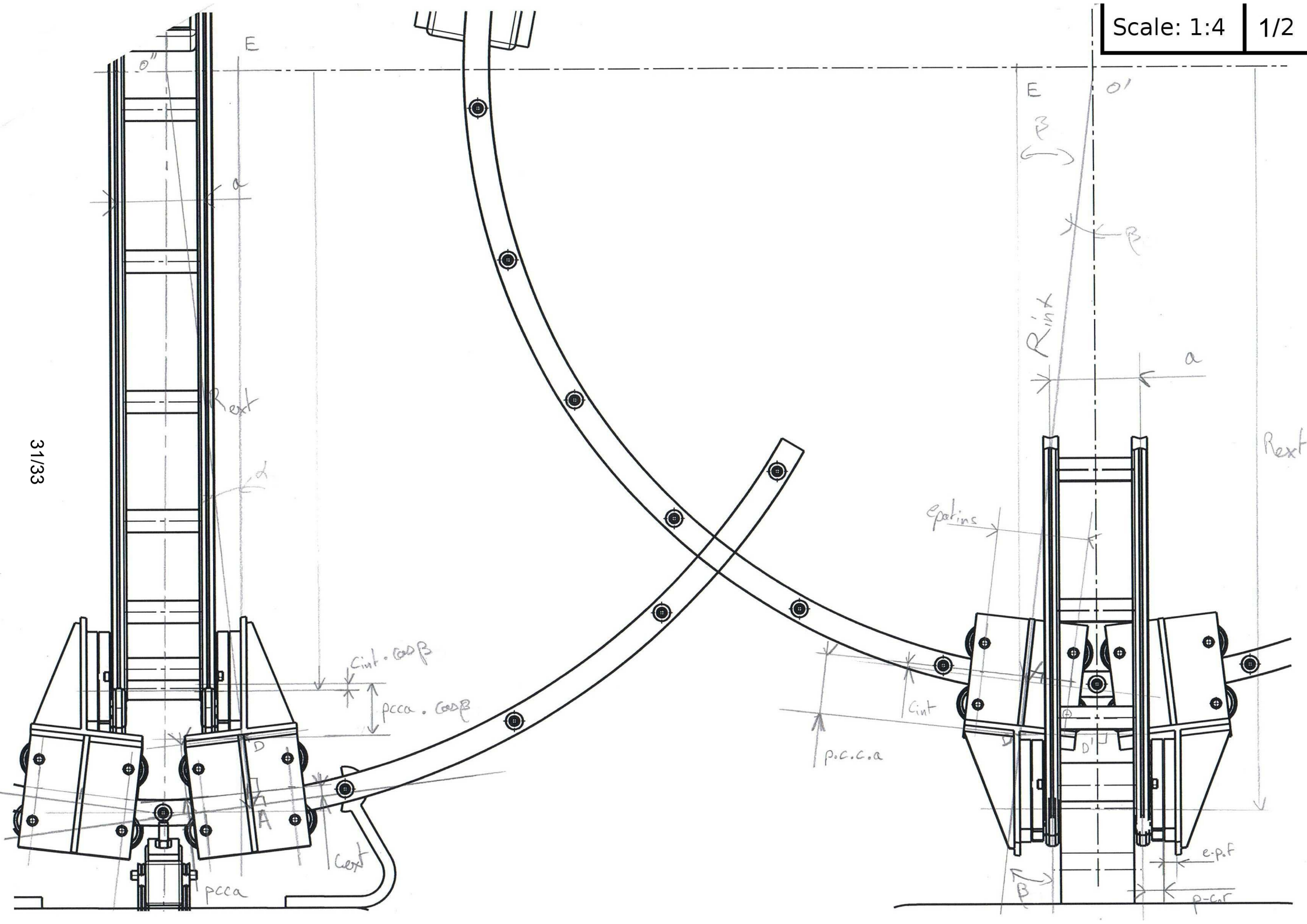
E
O''
a
Rext
d
Cint . cosβ
pcca . cosβ
D
A
Cext
pcca
E
O'
β
R
Rint
a
Rext
epfins
Cint
p.c.c.a
D'
e-p.f
p-car

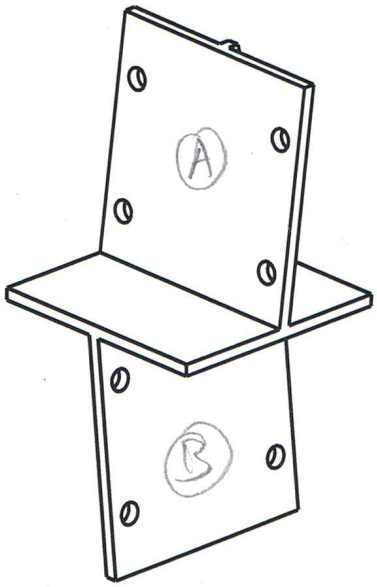

Vue isométrique
Echelle : 1:3

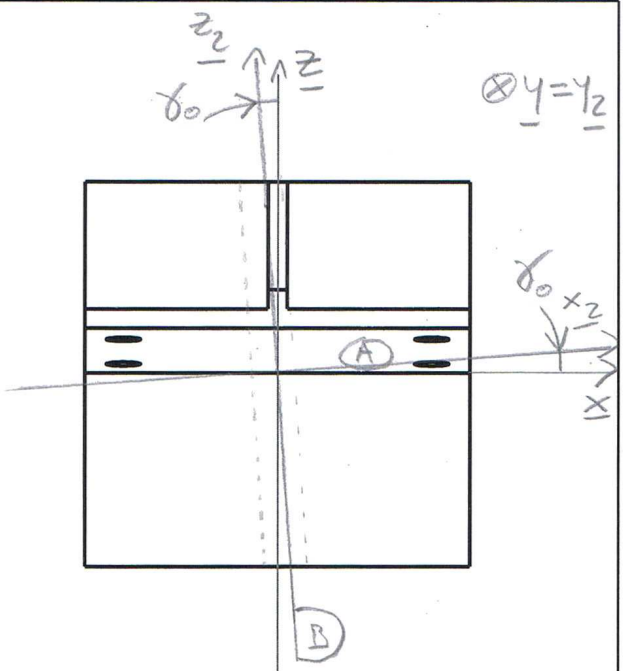

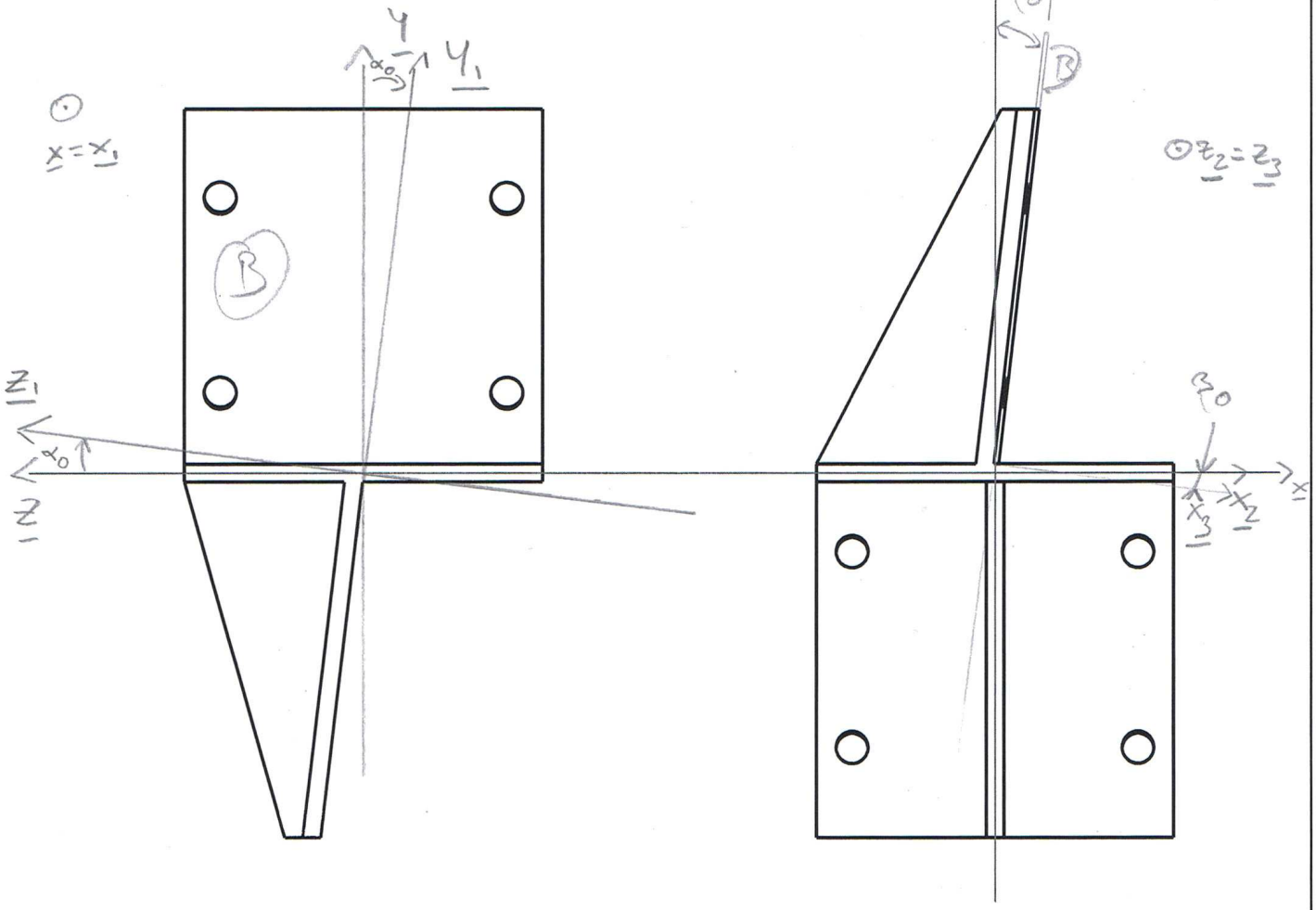

Mod.		13.12.2011	Mod.			Dessiné	11.2011	Laurent Blanchet	Echelle 1:2
						Contrôlé			
						Conf aux norm			
						Bon pour exéc.			
Sans nomenclature séparée ☒						N° de commande	PROTO		
Nomenclature sép de même N° ☐			Matiere	ABS		Origine		Format A4	Nb feuilles 2	Feuille N° 2
Nomenclature sép de N° diff ☐			Masse	0.196 kg		Remplace			

EPFL

Dénomination
A Link of the right-sided gliders

N° de dessin
Proto - RC

References

[1] Northern Sky Research. New NSR report projects over 1,600 satellites worth $250 billion to be launched over the next 15 years. Technical report, NSR, June 2011. Link to the article on www.nsr.com.

[2] Reto Wiesendanger. Clean-me: concept for an orbital debris removal mission : Preliminary evaluation. Seed-Money Activity, 2010. EPFL.

[3] Laurent Blanchet. Orbital debris remediation: an approach using a 7-dof robotic arm in space. Master's thesis, EPFL, 2011.

[4] K. Yoshida. Engineering test satellite VII flight experiments for space robot dynamics and control: Theories on laboratory test beds ten years ago, now in orbit. *International Journal of Robotics Research*, 22(5):321–335, 2003.

[5] Y. Xu and T. Kanade, editors. *Space Robotics: Dynamics and Control*. Kluwer Academic Publishers, 1993.

[6] Francois Caullier. DR.LEO - AOCS and rendezvous. Master's thesis, Cranfield University, 2010.

[7] K. Yoshida and Y. Umetani. *Space Robotics: Dynamics and Control*, chapter Control of Space Manipulators with Generalized Jacobian Matrix. Kluwer Academic Publishers, 1993.

[8] Kazuya Yoshida and Brian Wilcox. Space robots and systems. In *Springer Handbook of Robotics*, pages 1031–1063. 2008.

[9] Dragomir Nenchev, Yoji Umetani, and Kazuya Yoshida. Analysis of a redundant free-flying spacecraft/manipulator system. *IEEE Transactions on Robotics and Automation*, 8(1):1–6, 1992.

[10] Simon Hyde. Approach and control of uncooperative orbital debris. ESTEC (ESA) draft, 2010.

[11] Cranfield University. *Debris Removal in Low Earth Orbit*, June 2010. 1st European Workshop on Active Debris Removal, CNES HQ (Paris).

[12] Florian Sellmaier, Toralf Boge, Jörn Spurmann, Sylvain Gully, Thomas Rupp, and Felix Huber. On-Orbit servicing missions: Challenges and solutions for spacecraft operations. In *SpaceOps 2010 Conference*, 2010.

[13] Markus Schlotterer and Stephan Theil. Testbed for on-orbit servicing and formation flying dynamics emulation. In *AIAA Guidance, Navigation, and Control Conference 2010*, August 2010. Paper-Nr: AIAA 2010-8108.

[14] ROLLON. Curviline catalog.

[15] THK. R guide, model hcr. Linear Motion Catalog.